International Journal of Pharmaceutics 532 (2017) 547–554

Contents lists available at ScienceDirect

International Journal of Pharmaceutics

journal homepage: www.elsevier.com/locate/ijpharm

Research Paper

Effects of nerolidol and limonene on stratum corneum membranes: A probe EPR and fluorescence spectroscopy study

Sebastião Antonio Mendanha[a], Cássia Alessandra Marquezin[a], Amando Siuiti Ito[b], Antonio Alonso[a,*]

[a] Instituto de Física, Universidade Federal de Goiás, Goiânia, GO, Brazil
[b] Faculdade de Filosofia Ciências e Letras de Ribeirão Preto, Universidade de São Paulo, Ribeirão Preto, SP, Brazil

ARTICLE INFO

Keywords:
Stratum corneum
Nerolidol
Spin label
Fluorescence probe

ABSTRACT

The sesquiterpene nerolidol and the monoterpene limonene are potent skin-permeation enhancers that have also been shown to have antitumor, antibacterial, antifungal and antiparasitic activities. Because terpenes are membrane-active compounds, we used electron paramagnetic resonance (EPR) spectroscopy of three membrane spin labels combined with the fluorescence spectroscopy of three lipid probes to study the interactions of these terpenes with stratum corneum (SC) intercellular membranes. An experimental apparatus was developed to assess the lipid fluidity of hydrated SC membranes via the fluorescence anisotropy of extrinsic membrane probes. Both EPR and fluorescence probes indicated that the intercellular membranes of neonatal SC rats undergo a main phase transition at approximately 50 °C. Taken together, the results indicated that treatment with 1% nerolidol (v/v) caused large fluidity increases in the more ordered phases of SC membranes and that these effects gradually decreased with increasing temperature. Additionally, compared with (+)-limonene, nerolidol was better able to change the SC membrane dynamics. EPR and fluorescence data suggest that these terpenes act as spacers in lipid packaging and create increased lipid disorder in the more ordered regions and phases of SC membranes, notably leading to a population of probes with less restricted motion.

1. Introduction

Drug-delivery systems have emerged as a good alternative for drugs that must be administered in high doses and may therefore cause harmful side effects to patients. From this standpoint, drug delivery through the skin has received increasing attention because of its wide application area and low metabolism. However, this route of administration is highly dependent on the ability of the drug to diffuse through the skin, which is generally very low. This low drug diffusion is associated with the skin barrier function, which is conferred by the most superficial layer of the skin: the stratum corneum (SC). Several molecules have been developed to reversibly alter the barrier function of the SC to allow drugs to reach therapeutic concentrations in the bloodstream (Santos et al., 2011, 2012), especially terpenes (Herman and Herman, 2015; Jain et al., 2002; Narishetty and Panchagnula, 2004). For example, Narishetty and Panchagnula demonstrated that the permeation of zidovudine (AZT), the first anti-HIV compound approved for clinical use, across rat skin was significantly increased by the terpenes cineole, menthol, α-terpineol, menthone, pulegone and carvone (Narishetty and Panchagnula, 2004).

Terpenes are molecules extracted from natural oils that are widely used by the pharmaceutical industry and are classified as safe by the USA Food and Drug Administration (FDA). Recently, studies using a variety of dietary monoterpenes have shown that these molecules, in addition to being good permeation enhancers, also have antitumor (Crowell, 1999), antibacterial (Cantrell et al., 2001), antifungal (Oliva et al., 2003), antiparasitic (Arruda et al., 2005, 2009), antiviral (Cragg and Newman, 2003) and anti-inflammatory activities (Yamada et al., 2013). For example, the monoterpene limonene has been shown to have promising protective activities against established skin squamous cell carcinomas (Hakim et al., 2000). Additionally, the sesquiterpene nerolidol has been shown to exert a toxic effect against a human hepatoma cell line (HepG2), inhibiting cell proliferation at 10 μM after 24 or 48 h of incubation (Ferreira et al., 2012). Nerolidol has also demonstrated antibacterial and antifungal activities (Tao et al., 2013). Regarding the antiparasitic activity of these two terpenes, Arruda and co-workers showed that nerolidol and limonene were effective at inhibiting the growth of different *Leishmania* species. The researchers also reported that treatment with the terpenes limonene and nerolidol reduced the infection rates of *Leishmania amazonensis*-infected macrophages by 78%

* Corresponding author.
E-mail address: alonso@ufg.br (A. Alonso).

http://dx.doi.org/10.1016/j.ijpharm.2017.09.046
Received 26 June 2017; Received in revised form 11 September 2017; Accepted 16 September 2017
Available online 19 September 2017
0378-5173/

and 95%, respectively. Finally, they showed that *Leishmania amazonensis*-infected mice treated with limonene (intrarectally or topically) displayed a significant reduction in lesion size and parasite load (Arruda et al., 2005, 2009).

Spin-label electron paramagnetic resonance (EPR) spectroscopy has been used to analyze thermally induced changes in the dynamics of SC membranes, as well as the effects of several monoterpenes on these changes (Camargos et al., 2010; dos Anjos et al., 2007a,b; dos Anjos and Alonso, 2008). The spin labels used in these studies were some stearic acid derivatives (dos Anjos et al., 2007a,b) and the small probes TEMPO (dos Anjos and Alonso, 2008) and DTBN (Camargos et al., 2010). In this work, we also used two spin-labeled phosphatidylcholines; in one of them, the paramagnetic group doxyl is attached to the 5th carbon atom of the sn-2 stearoyl chain of the phospholipid (5-PC), and in the other, the choline of the headgroup bears the nitroxide moiety (PC-TEMPO). These two spin labels might reflect the phosphatidylcholine (the lipid base of several nanocarriers designed for topical application) behavior when it is structured in the SC lipid lamellae. In parallel, a detailed analysis was also conducted with the appropriate spin-labeled stearic acid having the nitroxide radical moiety (doxyl) at the 5th carbon atom of the acyl chain (5-DSA) and three additional fluorescence probes. The use of lipophilic extrinsic fluorescent probes is presented as an alternative to the use of autofluorescence to evaluate the interaction of SC with molecules of interest and allows a study directed to the SC lipid matrix. Previous studies demonstrated that the sesquiterpene nerolidol was more cytotoxic to cultured fibroblasts than seven monoterpenes (Mendanha et al., 2013) and showed a much higher leishmanicidal activity than the monoterpenes (+)-limonene, α-terpineol and 1,8-cineole (Camargos et al., 2014); thus, in the present study, we focused on comparing the effects of nerolidol on the lipid dynamics of SC membranes to those of (+)-limonene based on information provided by EPR and fluorescence spectroscopy.

2. Materials and methods

2.1. Chemicals

The phospholipid 1,2-dipalmitoyl-*sn*-glycero-3-phosphocholine (DPPC), the fluorescent probe 1-palmitoyl-2-{6-[(7-nitro-2-1,3-benzoxadiazol-4-yl) amino] hexanoyl}-*sn*-glycero-3-phosphocholine (6-NBD-PC), and the spin labels 1,2-dipalmitoyl-*sn*-glycero-3-phospho (tempo)choline (PC-TEMPO) and 1-palmitoyl-2-stearoyl-(5-doxyl)-*sn*-glycero-3-phosphocholine (5-PC) were purchased from Avanti Polar Lipids Inc. (Alabaster, USA). The fluorescent probe 1,6-diphenyl-1,3,5-hexatriene (DPH) was acquired from Life Technologies of Brazil Ltd. (São Paulo, Brazil), and the fluorescent probe 2-amino-*N*-hexadecyl benzamide (AHBA) was prepared as previously described by Marquezin et al. (2006). The spin label 5-doxyl-stearic acid (5-DSA) was acquired from Sigma Aldrich (St. Louis, USA). The terpenes nerolidol and (+)-limonene were purchased from Acros Organics (Geel, Belgium) (Fig. 1). Nerolidol was used as a mixture of cis and trans isomers, whereas limonene was used in its (R)-(+)-limonene isomer form. The purity of the terpenes nerolidol and limonene was ≥97.0% and 96%, respectively. All other reagents were purchased from Sigma Aldrich (St. Louis, MO, USA) or Merck SA (Rio de Janeiro, Brazil) at the highest available purity, and all of the solutions were prepared with MilliQ water.

2.2. SC membrane preparation

SC membranes were obtained from Wistar rats that were less than 24 h old and prepared according to the protocol described by Alonso et al. (1995, 2001), which was approved by the Ethics Committee for the use of animals in research at the Universidade Federal de Goiás (protocol number: 022/16). Briefly, after the animals were sacrificed, their skins were removed and separated from the residual fat. To isolate the SC membranes, the skins were placed in contact with ammonium hydroxide vapor for 5 min and then with distilled water for 2 h. Next, the skins were placed on filter papers, and the SC membranes were carefully separated from the epidermis. Then, the SC membranes were washed with distilled water and dried at room temperature. Finally, the membranes were stored in a desiccator under moderate vacuum with silica gel until use.

2.3. SC membrane labeling and treatment

Intact SC samples (~2 mg) were incubated for 30 min at room temperature in an acetate-buffered saline solution (10-mM acetate and 150-mM NaCl, pH 5.1). Then, the hydrated SC membranes were repeatedly rubbed in glass plates containing an aliquot (2 μL) of the desired fluorescent or spin probes (dissolved in ethanol at 5 mg/mL). Subsequently, the SC membranes were incubated for 90 min at room temperature in solutions containing terpene-ethanol/buffer (0.25–1% v/v; terpene-ethanol 1:2 v/v). The terpenes were first solubilized in ethanol at a 1:2 v/v (terpene:ethanol) ratio, and the desired volume of this terpene-ethanol solution was then added to the buffer to obtain (0.25–1% v/v) terpene-ethanol/buffer solutions. For EPR spectroscopy, the SC membranes were added to glass capillaries, which were sealed by flame; for fluorescence spectroscopy, the SC samples were placed between quartz plates and added to a quartz cuvette containing buffered solution. Under these conditions, the SC can be considered to be in its fully hydrated state during all of the measurements. This methodology has been used recently to study SC autofluorescence *ex vivo*, as well as the effects of nerolidol on the fluorescence photobleaching and quantum yield of exogenous and endogenous SC porphyrins (Alonso et al., 2016).

2.4. DPPC vesicle preparation and treatment

DPPC lipid films (dissolved in 1-mg/mL chloroform) containing the desired fluorescent probe (initially dissolved in ethanol) at a probe:lipid molar ratio of 1:100 were formed in glass tubes by evaporation of the solvent with a nitrogen gas flow. To remove residual organic solvent, the films were kept under vacuum for 12 h. Then, the lipid films were hydrated with 200 μL of saline phosphate buffer (5-mM phosphate and 150-mM NaCl, pH 7.4) to form a suspension of multilamellar DPPC vesicles. Unilamellar vesicles were prepared with a mini-extruder purchased from Avanti Polar Lipids Inc. equipped with a polycarbonate filter (pore diameter of 0.1 μm). Subsequently, the DPPC vesicles were cooled and concentrated by centrifugation (1000 × *g* at 4 °C, 10 min). The required aliquots of a stock solution containing terpenes diluted in ethanol to a terpene:ethanol ratio of 1:2 (v/v) were added to this suspension. To avoid light scattering effects, the final DPPC concentration was fixed at 0.2 mM.

2.5. Fluorescence anisotropy measurements

Steady-state fluorescence anisotropy measurements were performed using a Horiba Fluorolog® FL-3221 spectrofluorometer (Kyoto, Japan) equipped with polarizers in the excitation and emission channels and a type-L measuring system. The temperature of the samples was controlled using a Cientec heat pump (Charlton, Brazil). The excitation wavelengths were 330 nm, 460 nm and 360 nm for the AHBA, 6-NBD-PC and DPH probes, respectively. The fluorescence anisotropy was calculated according to the following equation (Weber et al., 1971):

$$r = \frac{I_{\parallel} - I_{\perp}}{I_{\parallel} + 2I_{\perp}} \quad (1)$$

where *r* is the steady-state fluorescence anisotropy, and $I_{||}$ and $I_{\perp}$ are the fluorescence intensities in the parallel and perpendicular directions, respectively, to the polarization plane of the excitation light for each

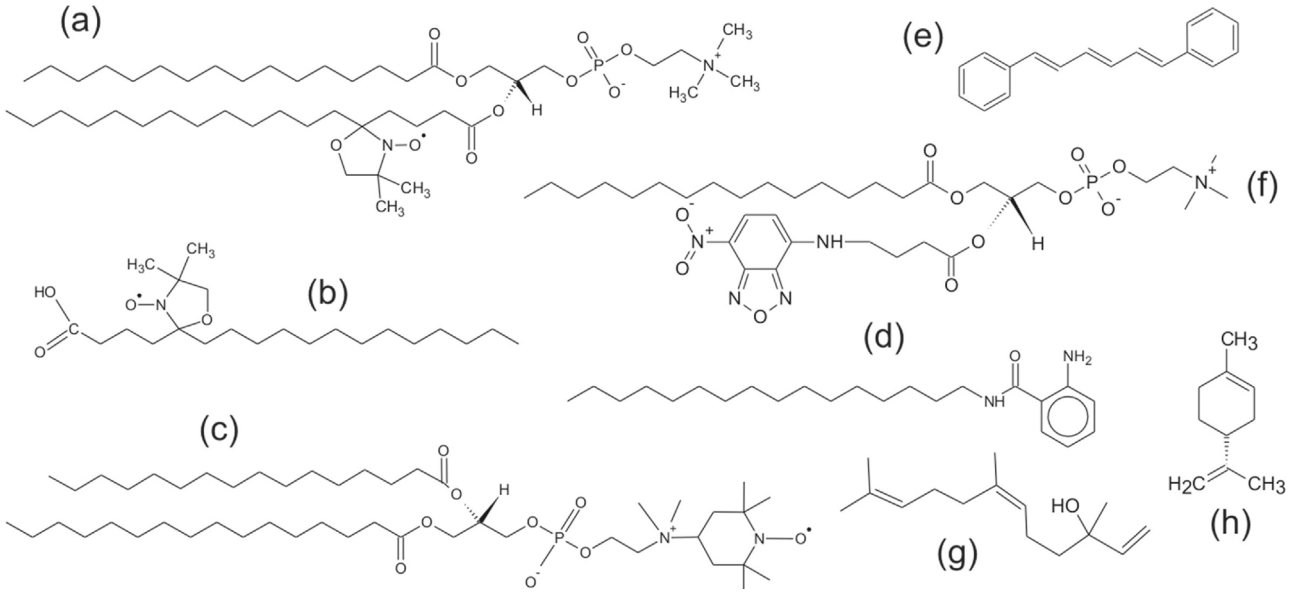

Fig. 1. Chemical structures of the terpenes, fluorescent probes and spin labels used in this work. AHBA and PC-TEMPO are presumed to monitor the polar interface of SC intercellular membranes. 6-NBD-PC, 5-PC and 5-DSA were used to monitor intermediate lipid regions, while DPH should monitor the deeper regions of the hydrophobic core. (a) 5-PC; (b) 5-DSA; (c) PC-TEMPO; (d) AHBA; (e) DPH; (f) 6-NBD-PC; (g) nerolidol (represented as its cis isomer) and (h) (R)-(+)-limonene.

wavelength used.

2.6. EPR spectroscopy measurements and spectral simulation

EPR measurements were performed using a Bruker EMX Plus spectrometer (Rheinstetten, Germany) operating in the X band (approximately 9.4 GHz) with a 4119 HS resonant cavity equipped with an Oxford MercuryiTC temperature controller (Abingdon, United Kingdom) and operating with the following instrumental parameters: microwave power, 2 mW; modulation frequency, 100 kHz; amplitude of modulation, 1 G; magnetic field scan, 100 G; scan time, 168 s; and detection time constant, 41 ms. The best fits to the EPR spectra were obtained using the nonlinear least-squares (NLLS) software developed by Freed JH and co-workers (Budil et al., 1996). As in other works (Mendanha and Alonso, 2015; Mendanha et al., 2013), the rate of rotational Brownian diffusion, R_{bar}, obtained from the NLLS program was converted to the rotational correlation time, τ_c, through the following relationship (Budil et al., 1996):

$$\tau_c = \frac{1}{6Rbar} \quad (2)$$

The best-fit spectra were calculated using models containing one or two spectral components (depending on the spin probe and the temperature range). All of the spectra were simulated using the same input parameters for the magnetic tensors g and A: $g_{xx}(1) = 2.0088$; $g_{yy}(1) = 2.0058$; $g_{zz}(1) = 2.0028$; $A_{xx}(1) = 6.6$; $A_{yy}(1) = 6.5$; $A_{zz}(1) = 33.0$; $g_{xx}(2) = 2.0088$; $g_{yy}(2) = 2.0058$; $g_{zz}(2) = 2.0026$; $A_{xx}(2) = 5.5$; $A_{yy}(2) = 5.5$; and $A_{zz}(2) = 30.8$; where the numbers (1) and (2) refer to the first and second spectral components, respectively. For the spectra fitted using the two-component model, the mean rotational correlation time was calculated as $\tau_c = (N_1{*}\tau_{c1} + N_2{*}\tau_{c2})/(N_1 + N_2)$, where N_1 and N_2 are the relative populations of spin labels present in components 1 and 2, respectively, provided by the NLLS software.

3. Results

3.1. Fluorescence spectroscopy of labeled SC and DPPC membranes

To validate the experimental apparatus used for the fluorescence anisotropy measurements of lipophilic probes embedded in the SC intercellular membranes, control experiments were performed to identify the best angles between the quartz plates and the sides of the cuvette that could ensure reproducibility of the fluorescence measurements. We note that this angle of orientation of the sample relative to the cuvette is not critical and can vary between 40 and 55° without essentially affecting the anisotropy values. In addition, parallel experiments with DPPC vesicles were also conducted to determine the standard behavior of the probes structured into lipid bilayers. This standardization allows us to determine whether the terpenes could alter the default behavior of the fluorescent probes and confirm that they had been correctly incorporated into the SC lipid phase.

The fluorescence emission spectra (at 25 °C) of the DPH probe incorporated into DPPC vesicles treated with nerolidol are shown in Fig. 2A. Because the addition of nerolidol did not significantly alter the band structure or the position of the emission spectra peaks for any of the three probes used in this work, the emission wavelengths used in the fluorescence anisotropy experiments were fixed at 400 nm, 527 nm and 427 nm for AHBA, 6-NBD-PC and DPH, respectively. In Fig. 2B, note that the DPH in DPPC vesicles showed the typical thermal

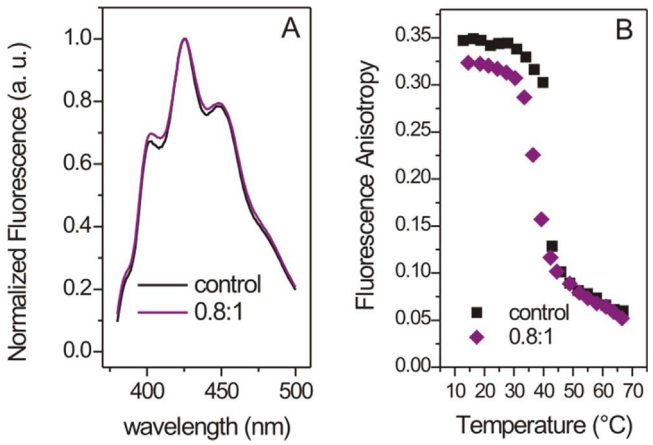

Fig. 2. Fluorescence emission spectra at 25 °C (Panel A) and fluorescence anisotropy profile as function of the temperature (Panel B) of DPH incorporated into DPPC vesicles treated with nerolidol at a 0.8:1 (terpene:lipid) ratio. The excitation wavelength used in both experiments was 360 nm.

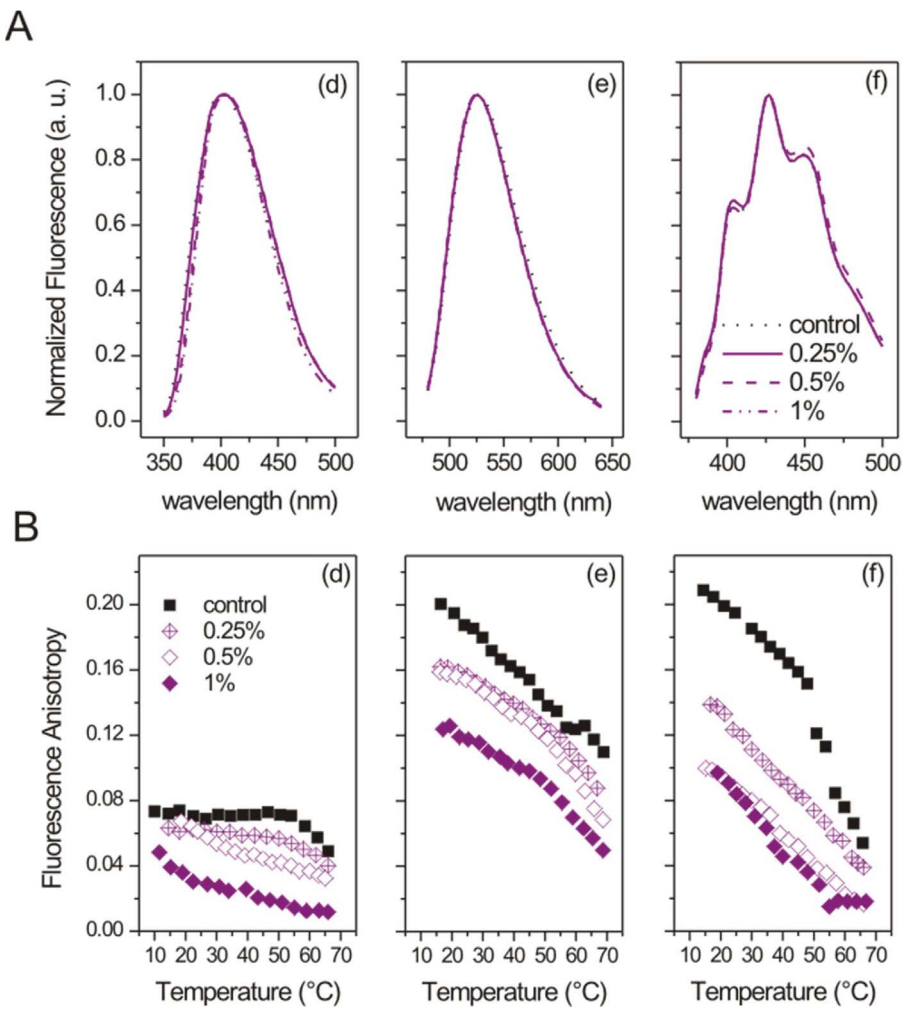

Fig. 3. Fluorescence emission spectra at 25 °C (Panel A) and fluorescence anisotropy profile as function of the temperature (Panel B) of different probes incorporated into SC membranes treated with 0.25, 0.5 and 1% nerolidol (v/v). The excitation wavelengths used in both experiments were 330 nm, 460 nm and 360 nm for AHBA, 6-NBD-PC and DPH, respectively. Inner panels: (a) and (d) AHBA; (b) and (e) 6-NBD-PC; and (c) and (f) DPH.

transition from the gel to lipid fluid phase occurring at 41 °C, as reported in the literature [see, *e.g.*, Ito et al., 2015]. With the addition of nerolidol, the DPH showed small increases in lipid fluidity below the major phase transition and no increase above the transition. Furthermore, the probe detected the reduction in the DPPC bilayer main phase transition temperature (by approximately 6 °C) upon nerolidol addition.

Fluorescence spectroscopy measurements of probes incorporated into the SC were performed with the SC membrane between quartz plates and added to a quartz cuvette (at an angle slightly less than 45° relative to the sides of the cuvette) containing a buffered solution. Fig. 3 shows that nerolidol essentially does not affect the emission spectra of probes incorporated into SC membranes (panel A) but significantly increases the molecular mobility (panel B). The addition of 0.25–0.5% (v/v) nerolidol was sufficient to suppress the SC phase transition monitored by the AHBA and DPH probes. For the samples labeled with 6-NBD-PC, the gradual increase in nerolidol concentration allowed better visualization of the phase transition, which was not well resolved in the control sample (without nerolidol treatment).

In Fig. 4, the DPH fluorescence anisotropy for SC samples treated with 1% (+)-limonene and nerolidol are compared. Treatment with the monoterpene leads to a decrease in the fluorescence anisotropy values compared with those of the control sample, although the phase transition starting from 45 to 50 °C remains unaltered. Note that the phase transition is completely suppressed by the nerolidol treatment, indicating that nerolidol has a greater ability to increase the dynamics of SC intercellular membranes than (+)-limonene.

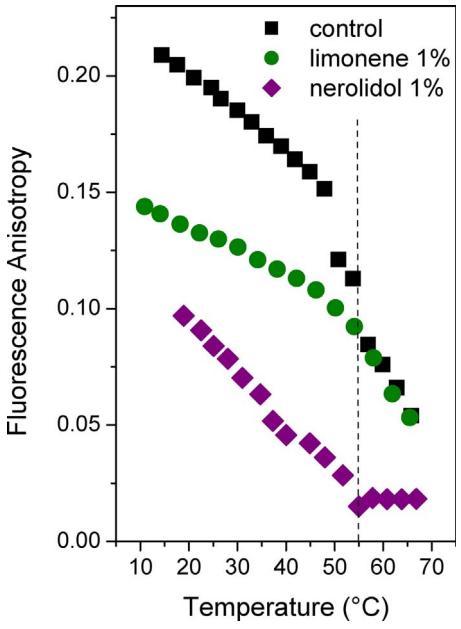

Fig. 4. Fluorescence anisotropy of the DPH probe incorporated into SC intercellular membranes as a function of temperature. Samples were treated with 1% (v/v) (+)-limonene or nerolidol for 90 min at 25 °C. The dotted vertical line indicates the first phase transition temperature (T_m ~55 °C) of the control sample (without terpene).

3.2. EPR spectroscopy of labeled SC membranes

The spectral profile of some spin labels incorporated in SC intercellular membranes can be fitted as the superposition of two spectral components with distinct line shapes and motion parameters (de Queirós et al., 2005; dos Anjos et al., 2007a,b). As discussed in previous works (Camargos and Alonso, 2013; Mendanha and Alonso, 2015), these two spectral components are associated with spin labels that assume one of two major localizations when incorporated into lipid bilayers. The principal component, namely, spectral component 1 (C1), is related to the fraction of the spin labels that strongly interact with the polar groups of the bilayer. This interaction leads to a broad line-shape profile, indicating slower and anisotropic molecular motion. In contrast, component 2 (C2) is related to the fraction of the spin labels that are more deeply inserted in the membrane hydrophobic core and therefore interact weakly with the polar interface. Spectral component 2 possesses narrower and less anisotropic lines as result of the higher degree of molecular movement. It has been demonstrated (Camargos and Alonso, 2013; Mendanha and Alonso, 2015) that the C1 and C2 spectral components can be assumed to be in a thermodynamic equilibrium and that the C2 resolution in the experimental spectrum is dependent on the temperature and fluidity of the system.

These two spectral components are illustrated in Fig. 5 for the spin label 5-DSA incorporated into intact and treated SC membranes. The spectrum of the control sample (without nerolidol treatment) can be fitted using just one spectral component. Note that as observed for several monoterpenes (dos Anjos et al., 2007a,b; Mendanha and Alonso, 2015), the treatment with 1% (v/v) nerolidol also alters the spin label distribution in favor of the C2 configuration and causes a distinct spectral line for this configuration in the experimental spectrum. Fig. 6 shows the spectra of the 5-DSA, 5-PC and PC-TEMPO spin labels incorporated into SC membranes. When 1% (v/v) nerolidol is added to the system, the spectral line shape of 5-DSA and 5-PC presents a resolved C2 feature over the entire temperature range. In contrast, the line shape of the PC-TEMPO spin label presents very smooth differences, and its spectra could be fitted using just one spectral component for 0–64 °C.

Fig. 7 shows the thermal behavior of the rotational correlation time, τ_c, obtained from the best-fit spectra of SC membranes labeled with the 5-DSA, 5-PC and PC-TEMPO spin probes in the form of Arrhenius plots of the natural logarithmic of τ_c as a function of the absolute temperature. The τ_c parameter reflects the molecular motion of the spin labels and has been used as a measurement of membrane fluidity (Alonso et al., 1995, 2012; Mendanha and Alonso, 2015). As shown, the addition of 1% (v/v) nerolidol to the SC membranes increases the lipid dynamics, leading to a decrease in the $\ln(\tau_c)$ values relative to those of the control samples from 0 to 50 °C. This decrease in the $\ln(\tau_c)$ values is related to the reduction in the temperature of the main phase transition of the SC membranes (also observed with the fluorescent probes) and to the increase in membrane fluidity. However, for temperatures above the main phase transition, the changes in the $\ln(\tau_c)$ values were small, indicating lower terpene effects, as monitored by the spin labels.

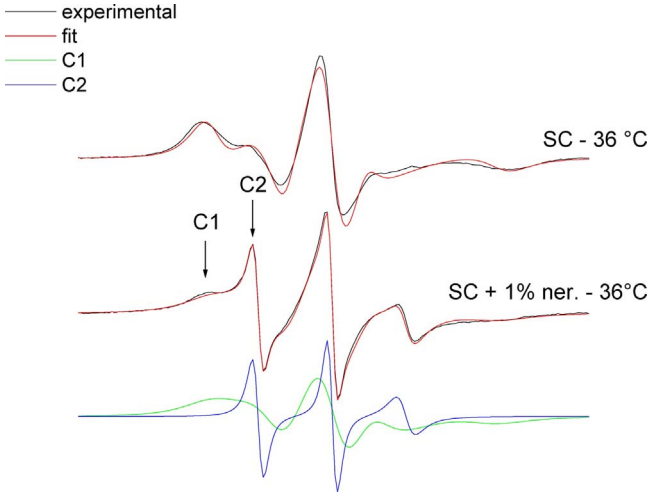

Fig. 5. Experimental (black lines) and best-fit (red lines) EPR spectrum of the spin label 5-DSA incorporated into SC membranes at 36 °C. The spin labels with more restricted molecular movement are generally attributed to component 1 (C1-green line), whereas the spin labels that are free to execute faster molecular movements are generally attributed to component 2 (C2-blue line). The arrows indicate the line-shape features of these components separated using the NLLS software. The addition of nerolidol mainly induces the spin label migration from C1 to C2. The total magnetic field range in each spectrum is 100 G (For interpretation of the references to colour in this figure legend, the reader is referred to the web version of this article.)

The Arrhenius plots shown in Fig. 7 allow the calculation of the activation energy, E_a, from the slopes of the curves of $\ln(\tau_c)$ *versus* 1/T using the equation (Alonso et al., 1995)

$$ln(\tau_c) = \frac{E_a}{RT} \tag{3}$$

where R is the gas constant, and T the absolute temperature. The values of E_a calculated using Eq. (3) are presented in Table 1. For the control samples, three distinct slopes are identified (with exception of the 5-PC spin label) over the measured temperature range, indicating that the spin probes experience three major energy barriers in their rotational motions. In contrast, when nerolidol was added to the SC membranes, the slope verified to occur from 20 to 30 °C is suppressed, and only two slopes could be identified. Note that for the 5-DSA and 5-PC spin probes, the addition of nerolidol to the bilayers decreases the values of E_a, suggesting that these two probes find more fluid environments. However, the addition of nerolidol does not significantly change E_a for PC-TEMPO. Interestingly, for PC-TEMPO that has the nitroxide moiety located outside the hydrophobic core of the membrane and close to the polar interface, an unexpected reduction in the rotational motion was observed in the temperature range of 50–64 °C (Fig. 7), suggesting that the more fluid phase favors a greater interaction of the nitroxide radical with the polar groups of SC membranes, thus reducing its movement.

4. Discussion

The SC has a distinct lipid composition from that of other cell membranes and has a complex lipid arrangement with three reported phase transitions. The first phase transition occurs from 55 to 65 °C (Gay et al., 1994) and is related to the loss of the orthorhombic crystalline structure of the lipids that are covalently bound to the exterior of the corneocyte envelope. The other two phase transitions occur at 72 °C and 83 °C (Bouwstra et al., 1991, 1992; Cornwell et al., 1996) and are associated with the scrambling of the lamellar phase (transition from the gel phase to the liquid crystalline phase). The latter two transitions disappear when the SC is delipidated (Cornwell et al., 1996), suggesting that these transitions are related to free lipids in the SC intercellular membrane that are not covalently bound to corneocytes (see the model described by Hill and Wertz, 2003). For the neonatal rat SC, the fluorescence anisotropy behaviors of the AHBA, 6-NBD-PC and DPH probes inserted into SC membranes as a function of temperature reflect the phase transition at approximately 50 °C. Above this temperature, the lipid dynamics are more temperature sensitive, and this behavior seems to decrease above 72 °C (Alonso et al., 1995; Camargos et al., 2010; dos Anjos and Alonso, 2008). Interestingly, this phase transition is well resolved for the AHBA and DPH probes but appears as only a slight change in slope for the 6-NBD-PC probe. Furthermore, the addition of nerolidol broadens the thermal phase transition observed with AHBA and DPH and increases the transition resolution of 6-NBD-PC.

The 6-NBD-PC probe, in which the fluorescent group is introduced in an intermediate position in the acyl chain, should be able to monitor the hydrophobic core of the membranes. However, the NBD polar group

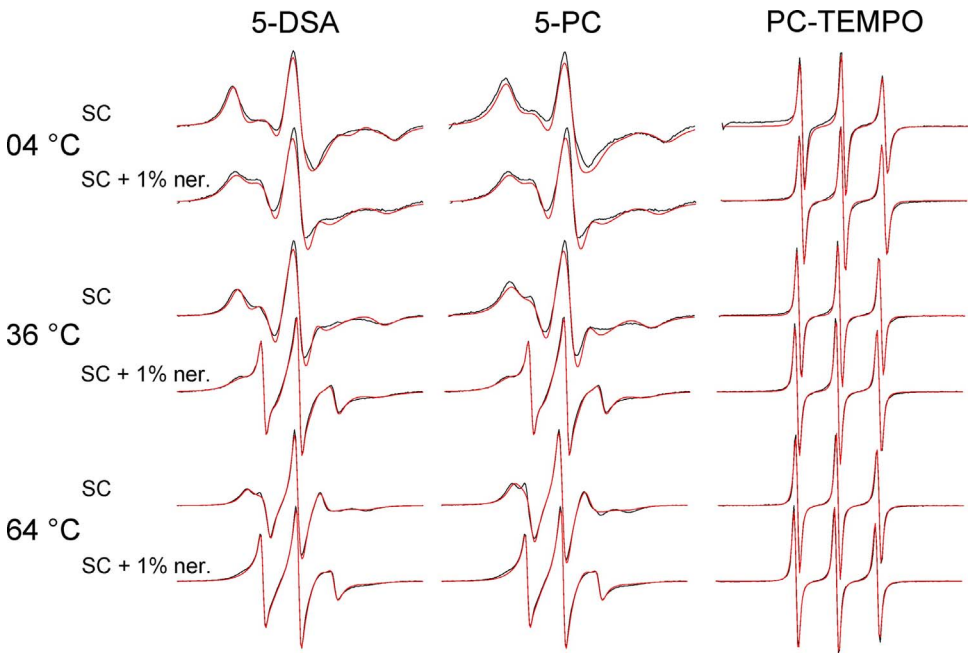

Fig. 6. Experimental (black lines) and best-fit (red lines) EPR spectra of the spin labels 5-DSA, 5-PC and PC-TEMPO incorporated into SC membranes at different temperatures. When SC membranes were treated with 1% (v/v) nerolidol, the population of spin labels that experience greater molecular movement (component 2) increased, and its contribution to the composite experimental line became more evident in the spectra of the 5-DSA and 5-PC spin labels. The total magnetic field range in each spectrum is 100 G (For interpretation of the references to colour in this figure legend, the reader is referred to the web version of this article.)

tends to move toward the water-lipid interface, as demonstrated by studies using molecular dynamics (Loura and Ramalho, 2007), fluorescence quenching (Abrams and London, 1993; Chattopadhyay and London, 1987) and steady-state and time-resolved fluorescence anisotropy techniques (Loura and Ramalho, 2007; Raghuraman et al., 2007). This behavior appears to be responsible for this probe's weak ability to reflect the first SC phase transition. Moreover, the presence of nerolidol appears to facilitate the entry of the NBD group into the membrane hydrophobic region, thereby increasing its sensitivity to phase transitions.

Similar to fluorescence anisotropy, the thermal behavior of the rotational correlation time associated with the 5-DSA, 5-PC and PC-TEMPO spin labels incorporated into SC membranes also reflects the first phase transition. The molecular structure of the probe and its location within the membrane also seem to be critical for the resolution of the phase transition. While 5-DSA and 5-PC, which have the nitroxide group positioned at the 5th carbon of their acyl chains, exhibited only slight phase transitions over the entire measured temperature range, PC-TEMPO, which has the nitroxide located at the outer polar surface of the membrane, showed a different thermal behavior in the temperature range of 50–64 °C (Fig. 7 and Table 1). This behavior suggests an interaction of the nitroxide with the polar groups of the membrane; this interaction increases with temperature between 50 and 64 °C.

The ability of terpenes to change the relative positions of the extrinsic probes inserted into SC membranes was demonstrated in previous work (dos Anjos et al., 2007b), where the addition of the monoterpene 1,8-cineole facilitated the transfer of fatty acid spin labels from being in contact with bilayer polar groups to being more deeply inserted in the membrane. A more recent study (Mendanha and Alonso, 2015) demonstrated that some terpenes, including nerolidol and (+)-limonene, not only anticipate the DPPC phase transition temperature but also facilitate the transfer of the spin labels 16- and 5-doxyl-stearic acid methyl ester between two locations within the DPPC bilayers. Moreover, terpenes can extract the spin labels from the membrane and transfer them to the solvent at higher concentrations. Above the DPPC main phase transition, nerolidol at a 0.8:1

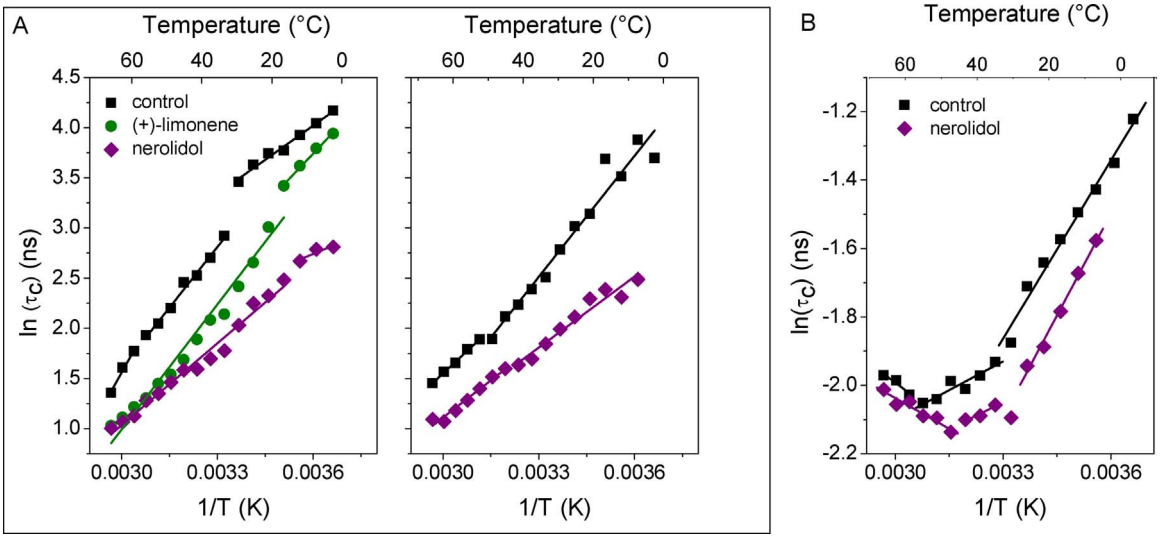

Fig. 7. Thermal behavior of the natural logarithmic of the rotational correlation time, τ_c, obtained through the NLLS best-fit of the 5-DSA, 5-PC (Panel A) and PC-TEMPO (Panel B) spectra of SC membranes at 0–64 °C. Arrhenius plots were used to calculate the activation energy (E_a) that the spin labels must overcome to have higher levels of molecular movement.

Table 1
Activation energies (calculated with eq. (3) and data showed into Fig. 7) of spin labels 5-DSA, 5-PC and PC-TEMPO structured into SC intercellular membranes.

	5-DSA			5-PC		PC-TEMPO		
	E_a (kcal/mol)			E_a (kcal/mol)		E_a (kcal/mol)		
	56–64 °C	28–52 °C	0–24 °C	48–64 °C	0–44 °C	52–64 °C	28–56 °C	0–24 °C
control	11.4	8.0	4.5	5.9	8.0	−1.6	1.1	3.4
	16–64 °C		0–12 °C	40–64 °C	0–36 °C	44–64 °C	28–40 °C	8–24 °C
nerolidol	5.4		2.8	4.9	4.7	−1.2	1.0	3.9
	16–64 °C		0–12 °C					
limonene	7.7		6.7					

terpene:DPPC molar ratio showed no significant effect on the lipid dynamics, which is in agreement with the results obtained for several monoterpenes using EPR spectroscopy (Camargos et al., 2010; dos Anjos and Alonso, 2008). However, in the case of the SC, the effects of the terpenes decreased with temperature but persisted up to high temperatures, in agreement with previous works using the small spin labels TEMPO (dos Anjos and Alonso, 2008) and DTBN (Camargos et al., 2010).

The addition of 0.25–0.5% nerolidol (v/v) makes the phase transition visualized by AHBA (which has its fluorescent group positioned near the polar groups of the bilayers) and DPH (which has non-polar characteristics) unobservable. Additionally, when incorporated into SC membranes, the fluorescence anisotropy of the AHBA probe is approximately 3 times lower than that observed in DPPC vesicles. As discussed by Marquezin et al. (2006), two rotational correlation times were identified for this probe when AHBA was incorporated into DMPC membranes. The larger of these times was associated with the rotation of the probe as a whole, while the shorter time was associated with the movement of its fluorescent aromatic ring. Recently, the emission anisotropy of fluorescent probes in lipid bilayers was examined, tracing a parallel between steady-state anisotropy and its time-averaged values, which are calculated from time-resolved anisotropy data (Ito et al., 2015). The steady-state anisotropy contains contributions from the rotational kinetics of the fluorophore, which reflect the environment fluidity, and from the residual anisotropy resulting from the structural restrictions imposed by the bilayer; the thermal phase transition observed in DPPC and DMPG vesicles using NBD probes reveal both aspects of the lipid organization (Ito et al., 2015). In contrast, the values of the limiting anisotropy of AHBA in DMPC vesicles are relatively low (Marquezin et al., 2006), implying their minor contribution to the steady-state anisotropy value, which is then mainly determined by the rotational correlation times. The results of this work suggest that AHBA is localized to a relatively fluid environment in SC membranes, leading to low rotational correlation times, and that the potential barrier that restricts the rotation of the probe is not so pronounced that it is experienced by the other probes. As a result, the AHBA probe displays lower anisotropy values than the other two probes in SC intercellular membranes.

Previous studies demonstrated that the sesquiterpene nerolidol is more cytotoxic to fibroblasts in culture than seven monoterpenes and showed a higher hemolytic potential (Mendanha et al., 2013). Furthermore, EPR spectroscopy has also been used to show that both nerolidol and (+)-limonene dramatically increase the molecular dynamics in *Leishmania amazonensis* promastigote plasma membranes at concentrations similar to their respective IC_{50} values (Camargos et al., 2014). This study also demonstrated that the sesquiterpene nerolidol induces more parasite lysis and is therefore more cytotoxic than (+)-limonene (IC_{50} value of 0.008 mM for nerolidol and 0.549 mM for (+)-limonene, Camargos et al., 2014). Overall, these data agree with the results obtained in this work and indicate that the *in vitro* cytotoxicity of terpenes is associated with their capacity to enhance membrane fluidity. These changes in cell membranes can lead to lysis of *Leishmania* parasites or leakage of K^+ ions in *Staphylococcus aureus* (Inoue et al., 2004). Thus, we suggest that this sesquiterpene could be used as an active compound for the treatment of cutaneous leishmaniosis, with an additional role as a skin-permeation enhancer in combination therapies with other antileishmanial agents.

5. Conclusions

The results of this work demonstrated that the fluorescence spectroscopy of lipophilic probes is sensitive enough to detect the effects of terpenes on the molecular order and mobility of SC lipids, similar to EPR spectroscopy, a more established technique for studying SC membranes. EPR and fluorescence data from several lipophilic probes indicated that neonatal rat SC membranes undergo a transition at approximately 50 °C. Other possible transitions were less clearly defined by these two techniques. In DPPC model membranes treated with nerolidol at a nerolidol:DPPC molar ratio of 0.8:1, the fluorescence probe DPH showed results consistent with spin-label EPR data from previous work. With both techniques, the probes showed that nerolidol increases the lipid dynamics of the DPPC bilayer at temperatures below the main phase transition and has no effect at temperatures above the transition. In contrast, treatment of the SC with 1% nerolidol caused an increase in membrane fluidity that was much more pronounced at low temperatures; however, the effect persisted throughout the measured temperature range. The effect of (+)-limonene at the same concentration was markedly less pronounced than that of nerolidol at temperatures below 30 °C. Based on the dynamics of the lipophilic probes, the action of the terpenes was always more pronounced in the more ordered membrane phases, and the EPR spectroscopy detected the formation of a population of probes with higher molecular dynamics. This behavior is consistent with the idea that nerolidol and (+)-limonene act as spacers for the membrane lipid chains and, particularly at higher temperatures, could have a higher concentration in the deeper regions of SC membranes.

Conflict of interest statement

The authors declare no conflicts of interest.

Acknowledgments

This work was financially supported by grants from the Brazilian research funding agencies CNPq, CAPES, FAPEG and FAPESP (2014/26895-7). Sebastião Antonio Mendanha was the recipient of a research grant from FAPEG (PPP03/2015). Antonio Alonso (CNPq303829/2016-8) and Amando Siuiti Ito (CNPq304981/2012-5) are recipients of research grants from CNPq. All of the EPR measurements were performed on the spectrometer installed at the EPR Laboratory (UnB) that was acquired though the research support of CNPq (CNPq573.880/2008-5 – INCT Nanobiotechnology).

References

Abrams, F.S., London, E., 1993. Extension of the parallax analysis of membrane penetration depth to the polar region of model membranes: use of fluorescence quenching by a spin-label attached to the phospholipid polar headgroup. Biochemistry 32, 10826–10831. http://dx.doi.org/10.1021/bi00091a038.

Alonso, A., Meirelles, N.C., Tabak, M., 1995. Effect of hydration upon the fluidity of intercellular membranes of stratum corneum: an EPR study. Biochim. Biophys. Acta 1237, 6–15. http://dx.doi.org/10.1016/0005-2736(95)00069-F.

Alonso, A., dos Santos, W.P., Leonor, S.J., dos Santos, J.G., Tabak, M., 2001. Stratum corneum protein dynamics as evaluated by a spin-label maleimide derivative: effect of urea. Biophys. J. 81, 3566–3576. http://dx.doi.org/10.1016/S0006-3495(01)75987-5.

Alonso, L., Mendanha, S.A., Marquezin, C.A., Berardi, M., Ito, A.S., Acuña, A.U., Alonso, A., 2012. Interaction of miltefosine with intercellular membranes of stratum corneum and biomimetic lipid vesicles. Int. J. Pharm. 434, 391–398. http://dx.doi.org/10.1016/j.ijpharm.2012.06.006.

Alonso, L., Marquezin, C.A., Gonçalves, P.J., Alonso, A., 2016. Transmittance and autofluorescence of neonatal rat stratum corneum: nerolidol increases the dynamics and partitioning of protoporphyrin IX into intercellular membranes. J. Fluoresc. 26, 709–717. http://dx.doi.org/10.1007/s10895-015-1758-z.

Arruda, D.C., D'Alexandri, F.L., Katzin, A.M., Uliana, S.R., 2005. Antileishmanial activity of the terpene nerolidol. Antimicrob. Agents Chemother. 49, 1679–1687. http://dx.doi.org/10.1128/AAC.49.5.1679-1687.2005.

Arruda, D.C., Miguel, D.C., Yokoyama-Yasunaka, J.K.U., Katzin, A.M., Uliana, S.R., 2009. Inhibitory activity of limonene against Leishmania parasites in vitro and in vivo. Biomed. Pharmacother. 63, 643–649. http://dx.doi.org/10.1016/j.biopha.2009.02.004.

Bouwstra, J.A., Gooris, G.S., van der Spek, J.A., Bras, W., 1991. Structural investigations of human stratum corneum by small-angle X-ray scattering. J. Invest. Dermatol. 97, 1005–1012. http://dx.doi.org/10.1111/1523-1747.ep12492217.

Bouwstra, J.A., Gooris, G.S., Vries, M.A.S., van der Spek, J.A., Bras, W., 1992. Structure of human stratum corneum as a function of temperature and hydration: a wide-angle X-ray diffraction study. Int. J. Pharm. 84, 205–216. http://dx.doi.org/10.1016/0378-5173(92)90158-X.

Budil, D.E., Lee, S., Saxena, S., Freed, J.H., 1996. Nonlinear-least-squares analysis of slow-motion EPR spectra in one and two dimensions using a modified Levenberg?Marquardt algorithm. J. Magn. Reson. Ser. A 120, 155–189. http://dx.doi.org/10.1006/jmra.1996.0113.

Camargos, H.S., Alonso, A., 2013. Electron paramagnetic resonance (EPR) spectral components of spin-labeled lipids in saturated phospholipid bilayers: effect of cholesterol. Quim. Nova 36, 815–821. http://dx.doi.org/10.1590/S0100-40422013000600013.

Camargos, H.S., Silva, A.H., Anjos, J.L., Alonso, A., 2010. Molecular Dynamics and partitioning of Di-tert-butyl nitroxide in stratum corneum membranes: effect of terpenes. Lipids 45, 419–427. http://dx.doi.org/10.1007/s11745-010-3407-2.

Camargos, H.S., Moreira, R.A., Mendanha, S.A., Fernandes, K.S., Dorta, M.L., Alonso, A., 2014. Terpenes increase the lipid dynamics in the leishmania plasma membrane at concentrations similar to their IC50 values. PLoS One 9, e104429. http://dx.doi.org/10.1371/journal.pone.0104429.

Cantrell, C.L., Franzblau, S.G., Fischer, N.H., 2001. Antimycobacterial plant terpenoids. Planta Med. 67, 685–694. http://dx.doi.org/10.1055/s-2001-18365.

Chattopadhyay, A., London, E., 1987. Parallax method for direct measurement of membrane penetration depth utilizing fluorescence quenching by spin-labeled phospholipids. Biochemistry 26, 39–45. http://dx.doi.org/10.1021/bi00375a006.

Cornwell, P.A., Barry, B.W., Bouwstra, J.A., Gooris, G.S., 1996. Modes of action of terpene penetration enhancers in human skin; differential scanning calorimetry, small-angle X-ray diffraction and enhancer uptake studies. Int. J. Pharm. 127, 9–26. http://dx.doi.org/10.1016/0378-5173(95)04108-7.

Cragg, G.M., Newman, D.J., 2003. Plants as a source of anti-cancer and anti-HIV agents. Ann. Appl. Biol. 143, 127–133. http://dx.doi.org/10.1111/j.1744-7348.2003.tb00278.x.

Crowell, P.L., 1999. Prevention and therapy of cancer by dietary monoterpenes. J. Nutr. 129, 775S–778S.

de Queirós, W.P., Neto, Dde S., Alonso, A., 2005. Dynamics and partitioning of spin-labeled stearates into the lipid domain of stratum corneum. J. Control. Release 106, 374–385. http://dx.doi.org/10.1016/j.jconrel.2005.05.009.

dos Anjos, J.L.V., Alonso, A., 2008. Terpenes increase the partitioning and molecular dynamics of an amphipathic spin label in stratum corneum membranes. Int. J. Pharm. 350, 103–112. http://dx.doi.org/10.1016/j.ijpharm.2007.08.024.

dos Anjos, J.L.V., Neto, Dde S., Alonso, A., 2007a. Effects of ethanol/l-menthol on the dynamics and partitioning of spin-labeled lipids in the stratum corneum. Eur. J. Pharm. Biopharm. 67, 406–412. http://dx.doi.org/10.1016/j.ejpb.2007.02.004.

dos Anjos, J.L., Neto, Dde S., Alonso, A., 2007b. Effects of 1, 8-cineole on the dynamics of lipids and proteins of stratum corneum. Int. J. Pharm. 345, 81–87. http://dx.doi.org/10.1016/j.ijpharm.2007.05.041.

Ferreira, F.M., Palmeira, C.M., Oliveira, M.M., Santos, D., Simões, A.M., Rocha, S.M., Coimbra, M.A., Peixoto, F., 2012. Nerolidol effects on mitochondrial and cellular energetics. Toxicol. In Vitro 26, 189–196. http://dx.doi.org/10.1016/j.tiv.2011.11.009.

Gay, C.L., Guy, R.H., Golden, G.M., Mak, V.H., Francoeur, M.L., 1994. Characterization of low-temperature (i.e., < 65 (C) lipid transitions in human stratum corneum. J. Invest. Dermatol. 103, 2393214. http://dx.doi.org/10.1111/1523-1747.

Hakim, I.A., Harris, R.B., Ritenbaugh, C., 2000. Citrus peel use is associated with reduced risk of squamous cell carcinoma of the skin. Nutr. Cancer 37, 161–168. http://dx.doi.org/10.1207/S15327914NC372_7.

Herman, A., Herman, A.P., 2015. Essential oils and their constituents as skin penetration enhancer for transdermal drug delivery: a review. J. Pharm. Pharmacol. 67, 473–485. http://dx.doi.org/10.1111/jphp.12334.

Hill, J.R., Wertz, P.W., 2003. Molecular models of the intercellular lipid lamellae from epidermal stratum corneum. Biochim. Biophys. Acta 1616, 121–126. http://dx.doi.org/10.1016/S0005-2736(03)00238-4.

Inoue, Y., Shiraishi, A., Hada, T., Hirose, K., Hamashima, H., Shimada, J., 2004. The antibacterial effects of terpene alcohols on Staphylococcus aureus and their mode of action. FEMS Microbiol. Lett. 237, 325–331. http://dx.doi.org/10.1016/j.femsle.2004.06.049.

Ito, A.S., Rodrigues, A.P., Moreira Pazin, W., Berardi Barioni, M., 2015. Fluorescence depolarization analysis of thermal phase transition in DPPC and DMPG aqueous dispersions. J. Lumin. 158, 153–159. http://dx.doi.org/10.1016/j.jlumin.2014.09.051.

Jain, A.K., Thomas, N.S., Panchagnula, R., 2002. Transdermal drug delivery of imipramine hydrochloride. I. Effect of terpenes. J. Control. Release 79, 93–101. http://dx.doi.org/10.1016/S0168-3659(01)00524-7.

Loura, L.M.S., Ramalho, J.P.P., 2007. Location and dynamics of acyl chain NBD-labeled phosphatidylcholine (NBD-PC) in DPPC bilayers. A molecular dynamics and time-resolved fluorescence anisotropy study. Biochim. Biophys. Acta 1768, 467–478. http://dx.doi.org/10.1016/j.bbamem.2006.10.011.

Marquezin, C.A., Hirata, I.Y., Juliano, L., Ito, A.S., 2006. Spectroscopic characterization of 2-amino-N-hexadecyl-benzamide (AHBA), a new fluorescence probe for membranes. Biophys. Chem. 124, 125–133. http://dx.doi.org/10.1016/j.bpc.2006.06.002.

Mendanha, S.A., Alonso, A., 2015. Effects of terpenes on fluidity and lipid extraction in phospholipid membranes. Biophys. Chem. 198, 45–54. http://dx.doi.org/10.1016/j.bpc.2015.02.001.

Mendanha, S.A., Moura, S.S., Anjos, J.L.V., Valadares, M.C., Alonso, A., 2013. Toxicity of terpenes on fibroblast cells compared to their hemolytic potential and increase in erythrocyte membrane fluidity. Toxicol. In Vitro 27, 323–329. http://dx.doi.org/10.1016/j.tiv.2012.08.022.

Narishetty, S.T.K., Panchagnula, R., 2004. Transdermal delivery of zidovudine: effect of terpenes and their mechanism of action. J. Control. Release 95, 367–379. http://dx.doi.org/10.1016/j.jconrel.2003.11.022.

Oliva, B., Piccirilli, E., Ceddia, T., Pontieri, E., Aureli, P., Ferrini, A.M., 2003. Antimycotic activity of Melaleuca alternifolia essential oil and its major components. Lett. Appl. Microbiol. 37, 185–187. http://dx.doi.org/10.1046/j.1472-765X.2003.01375.x.

Raghuraman, H., Shrivastava, S., Chattopadhyay, A., 2007. Monitoring the looping up of acyl chain labeled NBD lipids in membranes as a function of membrane phase state. Biochim. Biophys. Acta 1768, 1258–1267. http://dx.doi.org/10.1016/j.bbamem.2007.02.001.

Santos, P., Watkinson, A.C., Hadgraft, J., Lane, M.E., 2011. Formulation issues associated with transdermal fentanyl delivery. Int. J. Pharm. 416, 155–159. http://dx.doi.org/10.1016/j.ijpharm.2011.06.024.

Santos, P., Watkinson, A.C., Hadgraft, J., Lane, M.E., 2012. Influence of penetration enhancer on drug permeation from volatile formulations. Int. J. Pharm. 439, 260–268. http://dx.doi.org/10.1016/j.ijpharm.2012.09.031.

Tao, R., Wang, C.Z., Kong, Z.W., 2013. Antibacterial/antifungal activity and synergistic interactions between Polyprenols and other lipids isolated from Ginkgo biloba L. leaves. Molecules 18, 2166–2182. http://dx.doi.org/10.3390/molecules18022166.

Yamada, A.N., Grespan, R., Yamada, Á.T., Silva, E.L., Silva-Filho, S.E., Damião, M.J., de Oliveira Dalalio, M.M., Bersani-Amado, C.A., Cuman, R.K., 2013. Anti-inflammatory activity of Ocimum americanum L. Essential oil in experimental model of zymosan-induced arthritis. Am. J. Chin. Med. 41, 913–926. http://dx.doi.org/10.1142/S0192415X13500614.